Title: Increase of the oxygen vacancy component in bridgmanite with temperature
Author: Zhaodong Liu, Masaki Akaogi, Tomoo Katsura
Publication: Earth and Planetary Science Letters
Publisher: Elsevier
Date: 29 October 2018

This is an Accepted Manuscript of an article published by Elsevier in Earth and Planetary Science Letters on 29 October 2018, available online: https://doi.org/10.1016/j.epsl.2018.10.014

© 2018. This manuscript version is made available under the CC-BYNC-ND 4.0 license http://creativecommons.org/licenses/by-nc-nd/4.0/

Increase of the oxygen vacancy component in bridgmanite with temperature

Zhaodong Liu[1]*, Masaki Akaogi[2], Tomoo Katsura[1, 3]

[1]Bayerisches Geoinstitut, University of Bayreuth, 95440 Bayreuth, Germany

[2]Department of Chemistry, Gakushuin University, 171-8588 Tokyo, Japan

[3]Center for High Pressure Science & Technology Advanced Research, Beijing, 100094, China

* Corresponding author: Zhaodong Liu (zhaodong.liu@uni–bayreuth.de)

Abstract

The oxygen vacancy (OV, $MgAlO_{2.5}$) contents in bridgmanite with periclase and/or a calcium ferrite-type $MgAl_2O_4$-Mg_2SiO_4 phase (CF-phase) were investigated at temperatures of 1700, 2000, and 2400 K and a pressure of 27 GPa using an ultrahigh-pressure multi-anvil press. The OV content increases significantly with increasing temperature by consuming coexisting periclase and the charge-coupled (CC, $AlAlO_3$) component in bridgmanite. The increase in OV component at high temperature is promoted by its high entropy. The CC components increase largely with temperature compared with the OV content in bridgmanite coexisting with CF-phase and periclase because the partition coefficient of Mg and Al between bridgmanite and CF-phase approaches unity because of the mixing entropy. The partial molar volumes of OV and CC bridgmanite endmembers at ambient conditions were constrained to be 26.64 and 25.79 cm^3/mol, respectively, with densities of 3.428 and 3.955 g/cm^3. By assuming linear relationships between wave velocities and density, the OV component may therefore cause a velocity reduction by one order of magnitude larger than the CC component at constant Al content in bridgmanite. The concomitant increase and decrease in OV and CC contents with temperature enhance V_P and V_S reductions by 0.7% and 2.5% in addition to anharmonic effects. The OV component in bridgmanite in subducted slabs is zero because of low temperature, and the transport of water and argon trapped by the OV component into the lower mantle by bridgmanite is therefore not expected. The storage capacity of these volatiles in subducted slabs will thus be significantly lower than the warm ambient mantle. Since the OV component is expected to enhance diffusion creep, the present results may explain slab stagnation in the mid-mantle due to low OV contents at low temperature, and vertically straight plumes in the lower mantle due to high OV contents at high temperature.

Keywords: oxygen vacancy, bridgmanite, temperature, velocity, volatile, slab stagnation

1. Introduction

Bridgmanite is the major host phase of aluminum (Al) in the Earth's lower mantle (Irifune, 1994). The incorporation of Al can produce significant effects on the chemical and physical properties of bridgmanite, including iron oxidation (McCammon, 1997; Frost et al., 2004), Fe-

Mg partitioning (Frost and Langenhorst, 2002), elasticity (*e.g.,* Zhang and Weidner, 1999; Brodholt, 2000; Jackson et al., 2004; Walter et al., 2004, 2006), and electrical conductivity (*e.g.,* Xu et al., 1998; Yoshino et al., 2016). Al is incorporated into bridgmanite via formation of both charge-coupled (CC) and oxygen vacancy (OV) components in the forms of $AlAlO_3$ and $MgAlO_{2.5}$, respectively (Hirsch and Shankland, 1991). In the CC component, Al^{3+} ions occupy Mg^{2+} and Si^{4+} sites (A- and B-sites hereafter) in the orthorhombic perovskite structure, whereas they occupy only B-sites and create oxygen vacancies in the OV component. Bridgmanite containing an OV component is thought to be more compressible than that with a CC component, suggesting that the shallower part of the lower mantle may be significantly weaker than deeper regions (Brodholt, 2000). The OV component has also been suggested to reduce the creep strength of bridgmanite, which may account for the viscosity increase in the mid-mantle (Liu et al., 2017a). In addition, the presence of an OV component in bridgmanite may induce volatiles such as water (Navrotsky, 1999) and noble gases (Shcheka and Keppler, 2012) into the lower mantle. Hence, it is important to evaluate the OV contents in bridgmanite at relevant conditions for better understanding the physical and chemical properties of the Earth's lower mantle.

Previous high-pressure and high-temperature synthesis experiments (Navrotsky et al., 2003; Kojitani et al., 2007a) suggested that significant amounts of OV component may be present in aluminous bridgmanite at 27 GPa and 1873 K in MgO-saturated $MgSiO_3$-$MgAlO_{2.5}$ systems. These results were confirmed by ^{27}Al nuclear magnetic resonance spectroscopy (Stebbins et al., 2003), which indicated that Al preferentially substitutes for Si^{4+} in the B-sites. More recently, Liu et al. (2017a) found that bridgmanite synthesized from a glass starting composition of $En_{90}Brm_{10}$ (En: $MgSiO_3$ enstatite; Brm: $MgAlO_{2.5}$ brownmillerite) at 27 GPa and 2000 K contains 5.7 mol% OV component. This concentration is significantly higher than values of 2.5-4.5 mol% synthesized at a lower temperature of 1873 K and identical pressure

reported by Navrotsky et al. (2003) and Kojitani et al. (2007a), suggesting that temperature may affect the OV content in bridgmanite. A temperature effect was also observed by Andrault et al. (2007) based on a compression study of aluminous bridgmanite using a laser-heated diamond anvil cell (LHDAC): the bulk modulus of bridgmanite synthesized at 1800 K (272 GPa) is significantly higher than that at 2300 K (244 GPa). Because bulk modulus is believed to decrease with increasing OV content (Brodholt, 2000), the lower bulk modulus of bridgmanite synthesized at higher temperature should imply a positive correlation between the synthesis temperature and OV content. However, Andrault et al. (2007) were not able to determine OV content owing to very small sample sizes in the LHDAC. Temperature is the most essential parameter for mantle dynamics because it differs significantly between cold subducted slabs (~1000-1400 K) and ambient lower mantle (~2000-2300 K) (*e.g.*, Brown and Shankland, 1981; Kirby et al., 1996; Eberle et al., 2002). Nevertheless, the effect of temperature on the maximum OV content in bridgmanite remains unclear. Furthermore, it is important to note that both theoretical (Brodholt, 2000) and experimental studies (Walter et al. 2006; Andrault et al. 2007) has reported that the proportion of the OV component may decrease rapidly at pressures above 24-25 GPa, which was recently confirmed by Liu et al. (2017a). Thus, the pressure effect has already been established.

In the present study, we determined the maximum OV contents along with the CC content in bridgmanite both with and without MgO-rich phases in the $MgSiO_3$–$MgAlO_{2.5}$ and $MgSiO_3$–Al_2O_3 systems at temperatures of 1700, 2000, and 2400 K and a constant pressure of 27 GPa using a multi-anvil press with tungsten carbide anvils. The results presented here are used to discuss the complicated chemistry and elasticity of bridgmanite and the volatile storage capacity of the lower mantle.

2. Experimental methods

Five starting materials were prepared in the present study. Two glass starting compositions were $En_{90}Brm_{10}$ (the subscripted number represents mol%; En: $MgSiO_3$ enstatite; Brm: $MgAlO_{2.5}$ brownmillerite) and $En_{95}Cor_5$ (Cor: Al_2O_3 corundum), which potentially form a single bridgmanite phase with either of the OV and CC components, respectively, as the principle component. Glasses were prepared from oxide mixtures of reagent grade MgO, SiO_2, and Al_2O_3, fused at 2000 K for 30 min and quenched into ice water. We repeated this process three times to fabricate homogeneous glasses. We also prepared powdered mixtures composed of 70 wt.% orthopyroxene with either an $En_{95}Cor_5$ or $En_{90}Brm_{10}$ composition (synthesized at 3 GPa and 1400 K for 5 hours) with 30 wt.% MgO, to examine reaction equilibration of run products by synthesizing bridgmanite obtained via different synthetic routes. It is important to note that the resulting bridgmanite should coexist with periclase and be saturated with MgO in the case of these two starting materials. A fine-grained oxide mixture with an $En_{70}Brm_{30}$ composition was also prepared, so that bridgmanite coexists with another Al_2O_3-rich phase in addition to periclase.

The starting materials were loaded into a platinum (Pt) capsule, and heated to 800 K for 1 hour to minimize water content before welding. High-pressure and high-temperature experiments were conducted at temperatures of 1700, 2000, and 2400 K under a constant pressure of 27 GPa for 4 to 30 hours using a Cr_2O_3-doped MgO octahedron with an edge length of 7 mm and hard TF05 tungsten carbide anvils with a truncated edge length of 3 mm with a press load of 15 MN in a Kawai-type multi-anvil apparatus (IRIS-15) at the Bayerisches Geoinstitut, University of Bayreuth (Ishii et al., 2016). The cell assembly included a $LaCrO_3$ sleeve heater and MgO sleeve for accommodating the Pt capsule. Temperature was measured using a $W_{97}Re_3$–$W_{75}Re_{25}$ thermocouple positioned at the center of the heater and adjacent to the base of the Pt capsule. No pressure correction was applied to thermocouple emf.

Experimental pressures at high temperature were calibrated based on the solubility of Al_2O_3 in bridgmanite in equilibrium with corundum (Liu et al., 2016, 2017b).

Recovered samples were mounted in epoxy resin, ground to expose the central portion, and then polished using 0.25 μm diamond paste. Textural observations and chemical analyses of the recovered samples were performed using a LEO1530 scanning electron microscope (SEM) and JEOL JXA-8200 electron probe microanalyzer (EPMA) operating at an acceleration voltage of 15 kV and beam current of 5 nA with enstatite and forsterite as standards for Mg and Si, respectively, and corundum as a standard for Al. We also determined the composition of pure $MgSiO_3$ bridgmanite using the same settings as a benchmark analysis, and obtained an accurate Mg/Si ratio of 1.008 ± 0.005. Samples were extracted from the Pt capsules after compositional analysis. XRD profiles were collected over a span of approximately two hours. Phases in the samples were identified using a micro-focused X-ray diffractometer with a Co anode operated at an acceleration voltage of 40 kV and beam current of 500 μA. The $MgSiO_3$ bridgmanite was used as an external standard to calibrate the Bragg angle (2θ) of the instrument.

3. Results

Experimental conditions and run products are summarized in **Table 1**.

3.1. Phase assemblages

Fig. 1 shows the XRD patterns of all run products. These results show that the $En_{90}Brm_{10}$ and $En_{95}Cor_5$ starting glasses crystallized into a single bridgmanite phase. The mixtures of $En_{90}Brm_{10}$ plus MgO and $En_{95}Cor_5$ plus MgO crystallized into a phase assemblage of bridgmanite plus periclase. The $En_{70}Brm_{30}$ sample crystallized into bridgmanite, periclase, and

a CF-phase (calcium ferrite-type structure of $MgAl_2O_4$-Mg_2SiO_4). **Fig. 2** shows back-scattered electron (BSE) images of the corresponding products. In these images, bridgmanite appears as gray grains, typically 3-10 μm in dimension, and some micro-cracks occur on the surfaces. On the other hand, periclase appears as dark gray grains, and the CF-phase shows smooth outlines. Some amorphization occurs in some bridgmanite grains in the samples of **Figs. 2a, 2b,** and **2c** as shown by a relatively bright color compared with gray bridgmanite grains, which may be caused by exposure under the electron beam during SEM analysis. Nevertheless, grain boundaries of each phases were clearly visible in the run products.

3.2. Phase compositions

The compositions of bridgmanite and coexisting phases are listed in **Table 2**. We confirmed that all phases are fairly uniform in composition. In addition, the bridgmanite from $En_{90}Brm_{10}$ shows similar compositions with those from the mixture of $En_{90}Brm_{10}$ plus MgO, and the BSE images show that all phases have relatively clear grain boundaries. These observations suggest that chemical equilibrium was achieved in the experiments.

Fig. 3a presents variations of the OV and CC contents with temperature obtained using different starting compositions. The OV and CC contents were calculated from the following equation: $Mg_xAl_zSi_yO_{x+1.5z+2y} = y\ MgSiO_3 + (x - y)\ MgAlO_{2.5}$ (OV) + $(z - x + y)/2\ AlAlO_3$ (CC), and $x + y + z = 2$ (Liu et al., 2017a). In the case of the single bridgmanite made from $En_{90}Brm_{10}$, the OV content increases from 3.0 ± 0.8 mol% at 1700 K to 5.2 ± 0.7 mol% at 2000 K to 6.2 ± 0.9 mol% at 2400 K. In contrast, the CC content concomitantly decreases from 3.5 ± 0.4 mol% at 1700 K to 1.7 ± 0.5 mol% at 2400 K. For the mixture of $En_{90}Brm_{10}$ plus MgO, bridgmanite coexisting with periclase possesses essentially the same OV and CC contents as those without periclase within the analytical uncertainties. It is noted that periclase coexisting with bridgmanite contains small amounts of Al_2O_3 ranging from 0.79 ± 0.03 wt.% at 2000 K

to 1.20 ± 0.07 wt.% at 2400 K (**Table 2**). The inverse correlation between the OV and CC contents is a result of the constant total Al content in bridgmanite within the samples.

As expected, the OV contents in bridgmanite from both the $En_{90}Brm_{10}$ glass and $En_{90}Brm_{10}$ plus MgO are significantly higher than those in the samples obtained from the $En_{95}Cor_5$ glass at all temperatures (**Table 2**). The OV content synthesized from $En_{95}Cor_5$ plus MgO is 4.5 ± 1.0 mol% at 2400 K. This value is significantly higher than 1.0 ± 0.6 mol% obtained from $En_{95}Cor_5$ but lower than that of 6.2 ± 0.9 mol% obtained from $En_{90}Brm_{10}$ at the same temperature, again within the analytical uncertainties.

The OV and CC contents in bridgmanite coexisting with CF-phase and periclase from $En_{70}Brm_{30}$ increase from 2.9 ± 0.7 and 4.6 ± 0.6 mol% at 1700 K to 4.3 ± 0.9 and 7.3 ± 0.8 mol% at 2400 K, respectively (**Fig. 3b**).This increase of the CC component with temperature is different from the case without a CF-phase (**Fig. 3a)**. In contrast, the Al content in the CF-phase decreases with increasing temperature: the $MgAl_2O_4$ contents in the CF-phase are 76 ± 2, 64 ± 1, and 61 ± 1 mol% at 1700, 2000, and 2400 K, respectively (**Table 2**). The Al partitioning in these phases will be discussed in detail later.

3.3 Molar volume of OV- and CC-dominated bridgmanite

The molar volumes of the synthetic bridgmanite are listed in Table S1 in the Supplementary material. **Fig. 4a** shows the molar volumes of bridgmanite with an Al pfu (pfu: per formula units based on the total cation number of 2) of 0.1 against synthesis temperature. As mentioned above, the OV component dominates in the $En_{90}Brm_{10}$ samples with and without MgO, whereas the CC component dominates in the $En_{95}Cor_5$ samples, and are called the OV- and CC-dominated bridgmanite, respectively. The molar volume of the OV-dominated bridgmanite increases from 24.51 ± 0.05 cm^3/mol at 1700 K to 24.55 ± 0.05 cm^3/mol at 2000 K to 24.60 ± 0.05 cm^3/mol at 2400 K. The CC-dominated bridgmanite has a molar volume of 24.48 ± 0.06

and 24.51 ± 0.05 cm^3/mol at 1700 and 2400 K, respectively, and is thus insensitive to synthesis temperature. The increase of molar volume of the OV-dominated bridgmanite with temperature is supported by Brodholt (2000).

Fig. 4b shows the molar volumes of bridgmanite against the OV and CC content in our present and recent studies (Liu et al., 2017b). To distinguish the effect of the OV component on the molar volume, we first fitted the volumes of the CC-bearing but OV-absent bridgmanite to a linear function, and obtained $V\ (X) = 24.44 + (\mathrm{dV}/dX) \times X$, where V is the molar volume in cm^3/mol, and X is the CC content in mol%. Thus, the CC component increases the molar volume of bridgmanite at a rate of 0.0135 (4) cm^3/mol (The number in parentheses represents the standard deviation of the last digit). From these values, the molar volume and density of the hypothetical CC endmember are found to be 25.79 (5) cm^3/mol and 3.955 (8) g/cm^3, which are almost consistent with those estimated by Akaogi and Ito (1999).These two values are 5.5 (2)% larger and -3.7 (2)% smaller than pure $MgSiO_3$ bridgmanite, respectively (24.44 cm^3/mol and 4.108 g/cm^3). We subtracted the effect of the CC component from the OV-dominated bridgmanite to obtain the molar volume of the pure OV-dominated bridgmanite. By fitting, we obtained the following equation: $V(X)$ = 24.44 + 0.022 (1) × X. Thus, the OV component increases the molar volume of bridgmanite at a rate of 0.022 (1) cm^3/mol, which is larger by 6% than that of CC component. From these values, the molar volume and density of the hypothetical OV endmember are found to be 26.64 (10) cm^3/mol and 3.428 (13) g/cm^3, which are 9.0 (4)% larger and -16.2 (4)% smaller than pure $MgSiO_3$ bridgmanite. It is emphasized that the density of the OV component is particularly small, which is partly because of its larger molar volume but more importantly because of its smaller formula weight due to the oxygen vacancy. The molar weights of $MgSiO_3$, Al_2O_3 and $MgAlO_{2.5}$ are 100.39, 101.96 and 91.28 g/mol, respectively.

4. Discussion

4.1 Inverse correlations between OV and CC contents in bridgmanite

To interpret the inversely correlated variation of OV and CC contents with temperature in bridgmanite synthesized form $En_{90}Brm_{10}$, the variation of these two components can be expressed by the following reaction:

$$2MgO + AlAlO_3\ (CC) = 2MgAlO_{2.5}\ (OV) \quad (1)$$

Because some amount of the CC component is present in what should have been MgO-free samples of $En_{90}Brm_{10}$ at 1700 and 2000 K, there may also have been small amounts of periclase in these samples according to reaction (1). However, we did not find any periclase by XRD or BSE observations. It is possible that the amount of periclase may be too low to be detected by XRD, and that tiny periclase grains may have been polished out from the surface prior by SEM analysis. The Gibbs free energy of reaction of (1) can be written as:

$$2\mu_{\mathrm{MgO}}^{\mathrm{Pc}} + \mu_{\mathrm{AlAlO_3}}^{\mathrm{Brg}} = 2\mu_{\mathrm{MgAlO_{2.5}}}^{\mathrm{Brg}} \quad (2)$$

where $\mu_{\mathrm{MgO}}^{\mathrm{Pc}}$, $\mu_{\mathrm{Al_2O_3}}^{\mathrm{Brg}}$, and $\mu_{\mathrm{MgAlO_{2.5}}}^{\mathrm{Brg}}$ are the chemical potentials of MgO in periclase and $AlAlO_3$ and $MgAlO_{2.5}$ components in bridgmanite, respectively. We use the non-ideal solution model of the chemical compositions in bridgmanite. The chemical potentials in these components can be written as:

$$\mu_{\mathrm{MgO}}^{\mathrm{Pc}} = \mu^{\circ}{}_{\mathrm{MgO}}^{\mathrm{Pc}} + RT \ln a_{\mathrm{MgO}}^{\mathrm{Pc}} \quad (3)$$

$$\mu_{\mathrm{AlAlO_3}}^{\mathrm{Brg}} = \mu^{\circ}{}_{\mathrm{AlAlO_3}}^{\mathrm{Brg}} + RT \ln a_{\mathrm{AlAlO_3}}^{\mathrm{Brg}} \quad (4)$$

$$\mu_{\mathrm{MgAlO_{2.5}}}^{\mathrm{Brg}} = \mu^{\circ}{}_{\mathrm{MgAlO_{2.5}}}^{\mathrm{Brg}} + RT \ln a_{\mathrm{MgAlO_{2.5}}}^{\mathrm{Brg}} \quad (5)$$

where $\mu^{\circ Pc}_{MgO}$, $\mu^{\circ Brg}_{AlAlO_3}$, and $\mu^{\circ Brg}_{MgAlO_{2.5}}$ are the chemical potentials of the (hypothetical) endmembers of these three components, and a^{Pc}_{MgO}, $a^{Brg}_{AlAlO_3}$, and $a^{Brg}_{MgAlO_{2.5}}$ are their activities. By substituting Eqs. (3), (4), and (5) into Eq. (2), the standard state Gibbs free energy change of reaction (1) can be then expressed as:

$$\Delta G^0_{R1} = 2\mu^{\circ Brg}_{MgAlO_{2.5}} - 2\mu^{\circ Pc}_{MgO} - \mu^{\circ Brg}_{AlAlO_3} = 2RT \ln a^{Pc}_{MgO} + RT \ln a^{Brg}_{AlAlO_3} - 2RT \ln a^{Brg}_{MgAlO_{2.5}} \quad (6)$$

Based on the symmetric regular solution model (Thompson, 1967), the activities of $AlAlO_3$ and $MgAlO_{2.5}$ component in bridgmanite can be expressed as:

$$RT \ln a^{Brg}_{AlAlO_3} = RT \ln(X^{Brg}_{Al_2O_3} \cdot \gamma^{Brg}_{AlAlO_3}) = RT \ln X^{Brg}_{AlAlO_3} + W^{Brg}_{AlAlO_3}\left(1 - X^{Brg}_{AlAlO_3}\right)^2 \quad (7)$$

$$RT \ln a^{Brg}_{MgAlO_{2.5}} = RT \ln(X^{Brg}_{MgAlO_{2.5}} \cdot \gamma^{Brg}_{MgAlO_{2.5}}) = RT \ln X^{Brg}_{MgAlO_{2.5}} + W^{Brg}_{MgAlO_{2.5}}\left(1 - X^{Brg}_{MgAlO_{2.5}}\right)^2 \quad (8)$$

where $X^{Brg}_{MgAlO_{2.5}}$ and $X^{Brg}_{AlAlO_3}$, respectively, are the mole fraction of the $MgAlO_{2.5}$ and $AlAlO_3$ components in the bridgmanite; $\gamma^{Brg}_{MgAlO_{2.5}}$ and $\gamma^{Brg}_{AlAlO_3}$ are an effective coefficient for expressing the non-ideality of mixing; $W^{Brg}_{AlAlO_3}$ and $W^{Brg}_{MgAlO_{2.5}}$ are interaction parameters for the degree of the non-ideality of mixing. For reaction (1), from Raoult's law (Guggenheim, 1937), we assume the activity of the MgO component in periclase as its mole fraction ($a^{Pc}_{MgO} = X^{Pc}_{MgO}$). The Gibbs free energy change of reaction (1) can then be expressed as:

$$\Delta G^0_{R1} = -RT \ln \frac{\left(X^{Brg}_{MgAlO_{2.5}}\right)^2}{\left(X^{Pc}_{MgO}\right)^2 X^{Brg}_{AlAlO_3}} + W^{Brg}_{AlAlO_3}\left(1 - X^{Brg}_{AlAlO_3}\right)^2 - 2W^{Brg}_{MgAlO_{2.5}}\left(1 - X^{Brg}_{MgAlO_{2.5}}\right)^2 \quad (9)$$

Here we estimate W_1 and W_2 by an empirical method for the the non-ideality of solid solutions due to a mismatch of the component volumes using the following formula (Davies and Navrotsky, 1983; Akaogi and Ito, 1999):

$$W_{\mathrm{G}} = 100.8 \cdot \Delta V - 0.4 \text{ kJ/mol} \quad (10)$$

$$\Delta V = \frac{V_A - V_B}{(V_A + V_B)/2} \quad (11)$$

where V_{A} and V_{B} are the molar volumes of the larger and smaller components, respectively. We then obtain $W^{\mathrm{Brg}}_{\mathrm{AlAlO_3}}$ and $W^{\mathrm{Brg}}_{\mathrm{MgAlO_{2.5}}}$ values of 5.0 ± 0.2 and 8.0 ± 0.8 KJ/mol from the present molar volume results. As shown in **Fig. 5**, the derived ΔG^0_{R1} would decrease from 41 ± 8 KJ/mol at 1700 K to 26 ± 6 KJ/mol at 2000 K to 20 ± 10 KJ/mol at 2400 K for the reaction of $En_{90}Brm_{10}$. ΔG^0_{R1} for the mixture of $En_{90}Brm_{10}$ + MgO at 2000 (21 ± 10 KJ/mol) and 2400 K (18 ± 9 KJ/mol) are consistent with those without MgO within uncertainties. By fitting the present experimental data in the absence of a CF-phase to a linear function of $\Delta G^0_{R1} = \Delta H^0_{R1} - T\Delta S^0_{R1}$, we obtained $\Delta S^0_{R1} = -\left(\frac{\partial \Delta G^0_{R1}}{\partial T}\right)_P = 27 \pm 9$ J/mol·K. This result suggests that high temperatures promote the forward progression of this reaction and thereby increase the OV content by consuming the CC component and periclase.

4.2 Al partitioning in bridgmanite, periclase, and the CF-phase

The appearing periclase in addition to bridgmanite in the $En_{70}Brm_{30}$ sample can also be explained by the Eqs. (1) – (9), although periclase contains only a very trace amount of Al_2O_3. By using the compositions of bridgmanite from $En_{70}Brm_{30}$ and assuming the periclase contains pure MgO, we obtained the ΔG^0_{R1} values of 47 ± 7, 57 ± 5, and 63 ± 8 kJ·mol^{-1} at 1700, 2000, and 2400 K, respectively. The derived ΔS^0_{R1} is -23 ± 7 J/mol·K, suggesting that the CC component is more favoured at high temperature compared with the OV component in bridgmanite for the $En_{70}Brm_{30}$ sample (**Fig. 3b**).

The exchange of Al^{3+} between bridgmanite and the CF-phase is expressed by the reaction:

$$MgAl_2O_4\ (CF) + MgSiO_3\ (Brg) = Mg(MgSi)O_4\ (CF) + AlAlO_3\ (Brg) \quad (12)$$

This reaction (12) represents the exchange of Al and Si between the CF-phase and bridgmanite, and so the OV component is not included. Mg^{2+} and Si^{4+} in the CF-phase would substitute for two Al^{3+} in octahedral sites through a charge-coupled substitution, although the $Mg(MgSi)O_4$ (*i.e.*, Mg_2SiO_4) endmember CF-phase cannot exist in the lower mantle because it is less stable than the mixture of $MgSiO_3$ bridgmanite and MgO periclase (Kojitani et al., 2007b). The Gibbs free energy change for reaction (12) can be expressed as:

$$\Delta G^0_{\mathrm{R12}} = RT \ln a^{\mathrm{Brg}}_{\mathrm{MgSiO_3}} + RT a^{\mathrm{CF}}_{\mathrm{MgAl_2O_4}} - RT \ln a^{\mathrm{Brg}}_{\mathrm{AlAlO_3}} - RT \ln a^{\mathrm{CF}}_{\mathrm{Mg(MgSi)O_4}} \quad (13)$$

Reaction (12) can be regarded as two binary systems of $MgSiO_3$-Al_2O_3 and $MgAl_2O_4$-$Mg(MgSi)O_4$. The activity coefficients for those components in bridgmanite and CF-phase can be expressed as:

$$a^{\mathrm{Brg}}_{\mathrm{AlAlO_3}} = (X^{\mathrm{Brg}}_{\mathrm{AlAlO_3}} \cdot \gamma^{\mathrm{Brg}}_{\mathrm{AlAlO_3}})^2 \quad (14)$$

$$a^{\mathrm{Brg}}_{\mathrm{MgSiO_3}} = (\gamma^{\mathrm{Brg}}_{\mathrm{MgSiO_3}} \cdot \gamma^{\mathrm{Brg}}_{\mathrm{MgSiO_3}})^2 \quad (15)$$

$$a^{\mathrm{CF}}_{\mathrm{MgAl_2O_4}} = (X^{\mathrm{CF}}_{\mathrm{MgAl_2O_4}} \cdot \gamma^{\mathrm{CF}}_{\mathrm{MgAl_2O_4}})^2 \quad (16)$$

$$a^{\mathrm{CF}}_{\mathrm{Mg(MgSi)O_4}} = (X^{\mathrm{CF}}_{\mathrm{SiMg_2O_4}} \cdot \gamma^{\mathrm{CF}}_{\mathrm{Mg(MgSi)O_4}})^2 \quad (17)$$

The activity coefficients can be written as:

$$RT\ln\gamma^{\mathrm{Brg}}_{\mathrm{AlAlO_3}} = W^{\mathrm{Brg}}_{\mathrm{Al}}(1 - X^{\mathrm{Brg}}_{\mathrm{AlAlO_3}})^2 \quad (18)$$

$$RT\ln\gamma^{\mathrm{Brg}}_{\mathrm{MgSiO_3}} = W^{\mathrm{Brg}}_{\mathrm{Al}}(1 - X^{\mathrm{Brg}}_{\mathrm{MgSiO_3}})^2 \quad (19)$$

$$RT\ln\gamma^{\mathrm{CF}}_{\mathrm{Mg(MgSi)O_4}} = W^{\mathrm{CF}}_{\mathrm{SiAl}}(1 - X^{\mathrm{CF}}_{\mathrm{Mg(MgSi)O_4}})^2 \quad (20)$$

$$RT\ln\gamma^{\mathrm{CF}}_{\mathrm{MgAl_2O_4}} = W^{\mathrm{CF}}_{\mathrm{SiAl}}(1 - X^{\mathrm{CF}}_{\mathrm{MgAl_2O_4}})^2 \quad (21)$$

where $X^{CF}_{MgAl_2O_4}$ and $X^{CF}_{Mg(MgSi)O_4}$ are the mole fractions of $MgAl_2O_4$ and $Mg(MgSi)O_4$ in the CF-phase, respectively. ΔG^0_{R12} can be expressed as:

$$\Delta G^0_{R12} = -2RT\ln\frac{X^{CF}_{Mg(MgSi)O_4}X^{Brg}_{AlAlO_3}}{X^{CF}_{MgAl_2O_4}X^{Brg}_{MgSiO_3}} + 2W^{CF}_{SiAl}\left(1-2X^{CF}_{MgAl_2O_4}\right) + 2W^{Brg}_{Al}\left(2X^{Brg}_{AlAlO_3}-1\right) \quad (22)$$

We used Eqs. (10) and (11) to fit the molar volume data for the CF-phase obtained by Kojitani et al. (2007b), yielding W^{CF}_{SiAl} of 0.6 kJ·mol^{-1}. The derived ΔG^0_{R12} changes from 108 ± 6 kJ·mol^{-1} at 1700 K to 98 ± 5 kJ·mol^{-1} at 2000 K and to 109 ± 6 kJ·mol^{-1} at 2400 K. Because these changes are identical within experimental error, ΔS^0_{R12} is essentially zero within analytical uncertainties (1 ± 16 J/mol·K, **Fig. 5**). Thus, reaction (12) will proceed in the forward direction because of the entropy of mixing. As such, both Al_2O_3 and Mg_2SiO_4 should be present only as minor impurities in the bridgmanite and CF-phase, respectively, although their concentrations will increase with temperature.

Both experimental and thermodynamics results indicate that high temperatures promote the reaction of CC-bearing bridgmanite with coexisting periclase to form OV-rich bridgmanite and the total Al-content of bridgmanite coexisting with only periclase is nearly constant for $En_{90}Brm_{10}$ with and without MgO sample (**Fig. 3a**). In contrast, for bridgmanite with CF-phase and periclase, the addition of an external Al-reservoir in the form of a CF-phase induces a total Al increase with temperature (**Fig. 3b**). This increase Al at high temperature would favor the CC content and the OV content thus slightly increase or keep almost constant, which resulting the OV/CC molar ratio remains almost constant at 0.5-0.6 in the 1700-2400 K range. In summary, the OV component content increases with temperature, especially for bridgmanite coexistence with periclase without a CF-phase. An increase of the OV content with temperature is therefore expected to occur in peridotitic or pyrolitic bulk compositions (bridgmanite

coexisting with pericalse) rather than basaltic compositions (bridgmanite coexisting with stishovite and a CF-phase).

5. Implications

5.1 Effect of the OV and CC component with temperatures on the elasticity of bridgmantie

An increase in the OV content with temperature should cause a decrease in bulk modulus because of its low density at high temperature because that a more looser structure should has a capability to be more substantially compressed (Brodhlot, 2000). The isothermal bulk modulus of aluminous bridgmanite has been thoroughly investigated and the various reported values of aluminous bridgmanite with a pyrolitic Al composition (Al pfu = 0.1) range from 232 to 272 GPa (*e.g.*, Zhang and Weidner, 1999; Daniel et al., 2001; Walter et al., 2004, 2006; Andrault et al., 2001, 2007). This large variation in bulk moduli could be related to variable OV contents in bridgmanite in response to different temperature and/or pressure conditions. In addition to the temperature effect demonstrated in the present study, increasing pressure has been shown to largely decrease the OV content (Liu et al., 2017a). Andrault et al. (2007) demonstrated that aluminous bridgmanite synthesized at 2300 K has a significantly lower bulk modulus (244 GPa) compared with that at lower temperature of 1800 K (272 GPa), and that the bulk modulus of bridgmanite synthesized at high pressures of 47-56 GPa (272 GPa) is substantially higher than that at lower pressures of 23-37 GPa (236 GPa). The increase of the OV content with increasing temperature and decreasing pressure and possible low bulk modulus of the OV component could explain these results. It is apparent that varying the temperature and pressure during synthesis can significantly affect the defect chemistry and thereby elastic properties of bridgmanite. The differences of bulk moduli between 272 and 244

GPa and 272 and 236 GPa potentially causes variations in bulk sound velocity of 5 to 7%, which are extremely large from a seismological point of view.

Although elasticity studies of aluminous bridgmanite, especially OV-bearing bridgmanite, are scarce, we simply argue here that the elasticity of aluminous bridgmanite based on Birch's law (Brich, 1952), namely, the linear relationships between compressional wave velocity (V_P) and density. We also assume a linear relationship between shear wave velocity (V_S) and density. Jackson et al. (2004) reported V_P = 10.84 km/s and V_S= 6.47 km/s for polycrystalline $MgSiO_3$ bridgmanite and V_P = 10.75 km/s and V_S= 6.35 km/s for $Mg_{0.95}Al_{0.1}Si_{0.95}O_3$ bridgmanite under ambient conditions. As Jackson et al. (2004) argued, the shear modulus, G, decreases significantly by 4% for 5 mol% Al_2O_3 component, while the adiabatic bulk modulus, K_S, is not affected. As a result, V_S decreases substantially (-1.8%), whereas V_P decreases only slightly (-0.8%). The present study shows that the density of $Mg_{0.95}Al_{0.1}Si_{0.95}O_3$ bridgmanite is 4.101 g/cm^3 under ambient conditions, which is slightly higher by 0.8 % that that obtained by Jackson et al. (2004) (4.081 g/cm^3). This leads to an increase of V_P and V_S to 10.82 and 6.49 km/s, respectively. In the present study, the OV-dominated bridgmanite with the same amount of Al_2O_3, namely, $MgAl_{0.1}Si_{0.9}O_{2.95}$ should have a density of 4.035 g/cm^3, which is significantly lower by 1.9% than that of the CC component (4.112 g/cm^3). This leads to large velocity drops, namely, V_P = 10.58 and V_S = 6.02 km/s. This evaluation suggests that the OV component decreases velocities 14 times more strongly than the CC component compared with the $MgSiO_3$ bridgmanite endmember.

In a pyrolite composition, all Al would be contained in bridgmanite and a CF-phase is thus absent. In this case, the CC and OV components, respectively, decrease and increase from 3.5 to 1.6 mol% and from 3.0 to 6.4 mol% with increasing temperature from 1700 to 2400 K, as shown in the present study. These values suggest that the V_P and V_S of bridgmanite in a pyrolitic mantle decrease by -0.7% and -2.5% with increasing temperature from 1700 to 2400 K purely

due to a change in the Al substitution mechanism. Aizawa et al. (2004) reported the temperature dependence of the adiabatic bulk and shear moduli are -0.029 and -0.024 GPa/K, respectively. Katsura et al. (2010) suggested that thermal expansion of bridgmanite at the top of the lower mantle is 2×10^{-5} /K. These data suggest that V_P and V_S of bridgmanite decrease with increasing temperature from 1700 to 2400 K by -2.5% and -2.7%, respectively, because of anharmonic effects. The change in Al substitution mechanisms thus enhances V_P and V_S reduction with elevating temperature by 3% and 5% in comparison with the anharmonic effects.

5.2 Volatile storage in the warm ambient lower mantle and cold subducted slabs

The presence of OV in bridgmanite may provide storage sites to incorporate hydroxyl (Navrotsky, 1999, Murakami et al., 2002) and noble gases with suitable atomic radii such as argon (1.64 Å), neon (1.18 Å), and helium (0.90 Å) (Shcheka and Keppler, 2012), although hydroxyl storage in the lower mantle is still under debate (*e.g.*, Murakami et al., 2002; Litasov et al., 2003; Bolfan-Casanova et al., 2003). In a pyrolitic composition, bridgmanite contains as much as 5 mol% OV component at 27 GPa and 2000 K, which is enough to explain a maximum of 1 wt.% water and argon incorporated in bridgmanite in the uppermost part of the lower mantle (Murakami *et al.*, 2002; Litasov et al., 2003; Shcheka and Keppler, 2012), although this component will rapidly decrease with increasing depth (Liu et al., 2017a). The present results show that the OV content decreases with decreasing temperature (0.5 mol% per 100 K), and the volatile storage capacity should therefore decrease to almost zero in subducted slabs because their typical temperature is significantly lower by ~800 K than the warm ambient lower mantle (Eberle et al., 2002).

It is also important to consider that pyrolitic bridgmanite contains significant amounts of iron (Fe) in addition to Al, and that the oxidation of Fe would prefer to form the charge-coupled

402 $FeAlO_3$ component (Frost and Langenhorst, 2002). This fact may even decreased the OV
403 component in bridgmanite in the ambient lower mantle. Here, we consider Mg^{2+}, Fe^{2+}, Fe^{3+},
404 and Al^{3+} as the major cations in pyrolitic bridgmanite and found that bridgmanite will contain
405 about 3 ± 1 mol% OV and 6 ± 1 mol% CC ($FeAlO_3$ plus $AlAlO_3$) at 26 GPa and 1900-2000 K
406 by assuming a Fe^{3+} fraction to the total iron ($Fe^{3+}/\Sigma Fe$) of 60 % in a reduced lower mantle
407 (McCammon, 1997; Frost et al, 2004) and Fe^{3+} preferably substituting into the Mg^{2+} site in the
408 uppermost lower mantle (Fujino *et al.*, 2012). This small amount of OV component will thus
409 typically decrease to zero in cold subducted slabs because of a very low temperature. To fully
410 understand the volatile cycle in the lower mantle, further studies is required to clarify the
411 concentration of trivalent cation such as Fe^{3+} and Al^{3+}, the coexisting phases such as periclase
412 in the pyrolite mantle model and stishovite in the MORB model, and the redox environment
413 on the chemistry defects of bridgmanite.

414 **5.3 Explanation of mantle plumes and slab stagnation in the lower mantle.**

415 The rheological properties of bridgmanite are expected to control lower-mantle
416 dynamics due to its dominant abundance. Karato and Wu (1993) suggested that diffusion creep
417 should dominate bridgmanite creep. The OV component will increase atomic diffusivity in
418 bridgmanite because of oxygen vacancy and therefore soften the lower mantle. Recent seismic
419 tomography showed that mantle plumes are straight and vertical in the lower mantle, but bend
420 significantly in the upper mantle (French and Romanowicz, 2015). This implies that
421 bridgmanite is more effectively softened at high temperature than upper mantle minerals.
422 Nevertheless, the activation enthalpy of olivine dislocation creep is about 500 kJ/mol (*e.g.*,
423 Karato and Jung, 2003), whereas that of Si diffusion in bridgmanite is smaller, about 300
424 kJ/mol (Yamazaki et al., 2000; Dobson et al., 2008, Xu et al., 2011), which is against the
425 expectation from the shapes of plumes. However, since the vacancy concentration in
426 bridgmanite will increase with temperature, diffusion creep should be more enhanced than

expected from the activation enthalpy of Si diffusion because of the OV component. Our conclusion of the present study, namely the positive temperature dependence of the OV content, may therefore explain seismic observations regarding mantle plumes.

Fukao and Obayashi (2013) depicted slab stagnation in the mid-mantle down to 1000-km depth. Similar to the discussion above, a nearly absent OV component should lead to much stiffer subducted slabs than the ambient mantle down to 1000 km because of the low temperature, which facilitates slab penetration into the lower mantle. However, the OV content in the ambient mantle also becomes nearly zero in deeper regions because of the negative pressure dependence of the OV content. The loss of viscosity contrast should impede slab subduction into the deep lower mantle and lead to slab stagnation in the mid-mantle. Our study thus provides an additional explanation for the seismically-observed slab stagnation in the mid-mantle.

6. Conclusions

We have clarified the temperature dependence of the OV content of bridgmanite in the presence of periclase without or with a CF-phase. In bridgmanite without a CF-phase, the OV content significantly increases with temperature by consuming the CC component and periclase as a result of the constant Al content. In bridgmanite coexisting with a CF-phase and periclase, the OV increase largely relative to the OV compoents with temperature by the supply of Al from the CF-phase. The formation of the OV component from the CC component and periclase is favored at high temperature, whereas the supply of Al from the CF-phase to bridgmanite is due to the entropy of mixing. The present results can explain the lower bulk modulus of bridgmanite synthesized at higher temperatures and lower pressures, which results from the high proportion of an OV component. The derived molar volume of the OV bridgmanite endmember is 26.64

451 cm^3/mol, which is 4 % higher than that of CC-endmember bridgmaite (25.79 cm^3/mol) at
452 ambient conditions. The OV component may thus cause lower velocities than the CC
453 component at constant Al content in bridgmanite. Bridgmanite in the uppermost of the ambient
454 lower mantle could contain significant amounts of volatiles such as noble gases and water. The
455 storage capacity of volatiles in bridgmanite in subducted slabs should be significantly lower
456 than that in the surrounding ambient mantle because of the lower slab temperatures.
457 A reduced of OV component with decreasing temperature can cause an increase in
458 the viscosity of bridgmanite from the warm ambient lower mantle to the surrounding cold
459 subducted slabs. This fact may explain seismically observed slab stagnation and vertically
460 straight plumes in the lower mantle. The present study helps to elucidate the complex chemistry
461 of bridgmanite and is therefore important for understanding the geophysics and geochemistry
462 of the Earth's lower mantle.

463

464 **Acknowledgements**

465 The authors thank D. Krauße for his technical assistance in electron microprobe analysis, and
466 E. S. Posner, H. Fischer and S. Übelhack for their assistance with high-pressure assembly
467 preparation. We also thank D. J. Frost for his discussion. The manuscript is greatly improved
468 by the constructive comments by R. G. Trønnes and an anonymous reviewer and the editorial
469 handling by J. P. Brodholt. Z. L. was financially supported by the Bayerisches Geoinstitut
470 Visitor's Program. This study is also supported by research grants to T. K. (BMBF: 05K13WC2,
471 05K13WC2; DFG: KA3434/3-1, KA3434/7-1, KA3434/8-1, KA3434/9-1).

472

473 **References**

474 Akaogi, M. and Ito, E., 1999. Calorimetric study on majorite–perovskite transition in the system
475 $Mg_4Si_4O_{12}$–$Mg_3Al_2Si_3O_{12}$: transition boundaries with positive pressure–temperature slope. Phys.
476 Earth Planet. Inter. 114, 129-140.

477 Aizawa, Y., Yoneda, A., Katsura, T., Ito, E., Saito, T., Suzuki, I., 2004. Temperature derivatives of
478 elastic moduli of $MgSiO_3$ perovskite. Geophys. Res. Lett. , 31(1).

479 Andrault, D., Bolfan–Casanova, N., Guignot, N., 2001. Equation of state of lower mantle (Al, Fe)–
480 $MgSiO_3$ perovskite, Earth Planet. Sci. Lett. 193, 501–508.

481 Andrault, D., Bolfan–Casanova, N., Bouhifd, M.A., Guignot, N., Kawamoto, T., 2007. The role of Al-
482 defects on the equation of state of Al-(Mg, Fe)SiO_3 perovskite. Earth Planet. Sci. Lett. 263, 167–
483 179.

484 Birch F., 1952. Elasticity and constitution of the Earth's interior J. Geophys. Res. 57, 227-286.

485 Brodholt, J. P., 2000. Pressure-induced changes in the compression mechanism of aluminous perovskite
486 in the Earth's mantle, Nature 407, 620–622.

487 Brown, J. M. and Shankland, T. J. Thermodynamic parameters in the Earth as determined from seismic
488 profiles. *Geophys. J., R. Astron. Soc.* **66**, 579–596 (1981).

489 Bolfan-Casanova N., Keppler, H., Rubie, D. C., 2003. Water partitioning at 660 km depth and evidence
490 for very low water solubility in magnesium silicate perovskite. Geophys. Res. Lett. 30, 1905.

491 Davies, P.K., Navrotsky, A., 1983. Quantitative correlations of deviations from ideality in binary and
492 pseudo-binary solid solutions. J. Solid State Chem. 46, 1–22.

493 Daniel, I. H. Cardon, H., Fiquet, G., Guyot, F., Mezouar, M., 2001. Equation of state of Al-bearing
494 perovskite to lower mantle conditions, Geophys. Res. Lett. 28, 3789–3792.

495 Dobson, D.P., Dohmen, R., Weidenbeck, M., 2008. Self-diffusion of oxygen and silicon in $MgSiO_3$. Earth
496 Planet. Sci. Lett.270, 125–129.

497 Eberle, M. A., Grasset, O., Sotin, C., 2002. A numerical study of the interaction between the mantle
498 wedge, subducting slab, and overriding plate. *Phys. Earth Planet. Inter.* 134, 191–202.

499 French, S. W., and B. Romanowicz, 2015, Broad plumes rooted at the base of the Earth's mantle beneath
500 major hotspots, *Nature*, 525 (7567), 95–99

501 Frost, D. J., and Langenhorst, F., 2002. The effect of Al_2O_3 on Fe–Mg partitioning between
502 magnesiowüstite and magnesium silicate perovskite. Earth Planet. Sci. Lett. 199, 227–241.

503 Frost, D. J., Liebske, C., Langenhorst, F., McCammon, C.A., Tronnes, R.G., Rubie, D.C., 2004.
504 Experimental evidence for the existence of iron-rich metal in the Earth's lower mantle. Nature
505 428,409–412.

506 Fujino, K., et al., 2012, Spin transition of ferric iron in Al-bearing Mg-perovskite up to 200 GPa and its
507 implication for the lower mantle, Earth Planet. Sci. Lett., 317–318, 407–412.

508 Fukao, Y., Obayashi, M. (2013) Subducted slabs stagnant above, penetrating through, and trapped
509 below the 660 km discontinuity. Journal of Geophysical Research: Solid Earth 118, 2013JB010466.

510 Guggenheim, E.A., 1937. Theoretical basis of Raoult's Law. Trans Faraday Soc 33, 151-I 59.

511 Hirsch, L. M., Shankland, T. J., 1991. Point defects in silicate perovskite. Geophys. Res. Lett. 18, 1305–
512 1308.

513 Horiuchi, H., Ito, E., Weidner, D. J., 1987. Perovskite-type MgSiO3: Single-crystal X-ray diffraction
514 study. Am. Mineral. 72, 357-360.

515 Irifune, T., 1994. Absence of an aluminous phase in the upper part of the Earth's lower
516 mantle, Nature 370 (6485), 131–133.

517 Ishii, T., et al., 2016. Generation of pressure over 40 GPa using Kawai–type multi–anvil press with
518 tungsten carbide anvils. Rev. Sci. Instr. 87, 024501–1–024501–6.

519 Jackson, J., Zhang, M., J. & Bass, J. D., 2004. Sound velocities and elasticity of aluminous $MgSiO_3$
520 perovskite: Implications for aluminum heterogeneity in Earth's lower mantle. Geophys. Res. Lett.
521 31, L10614.

522 Karato, S., Wu, P., 1993. Rheology of the upper mantle: a synthesis. Science 260, 771–778.

523 Karato, S., Jung, H., 2003. Effects of pressure on high-temperature dislocation creep in olivine. Phil
524 Mag 83:401–414

525 Katsura, T., Yoneda, A., Yamazaki, D. et al., 2010. Adiabatic temperature profile in the mantle. Phys.
526 Earth Planet Inter. 183, 212–218.

527 Kirby, S. H., Stein, S., Okal, E. A., & Rubie, D. C., 1996. Metastable mantle phase transformations and
528 deep earthquakes in subducting oceanic lithosphere. Rev. of Geophys. **34**(2), 261–306

529 Kojitani, H., Katsura, T., Akaogi, M., 2007a. Aluminum substitution mechanisms in perovskite-type
530 $MgSiO_3$: An investigation by Rietveld analysis. Phys. Chem. Miner. 34, 257–267.

531 Kojitani, H., R. Hisatomi, Akaogi, M., 2007b, High-pressure phase relations and crystal chemistry of
532 calcium ferrite-type solid solutions in the system $MgAl_2O_4$-Mg_2SiO_4, *Am. Mineral., 92*, 1112-1118

533 Litasov, K., Ohtani, E., Langenhorst, F., Yurimoto, H., Kubo, T., Kondo, T. 2003. Water solubility in
534 Mg-perovskites and water storage capacity in the lower mantle. Earth Planet. Sci.
535 Lett. 211(1), 189–203.

536 Liu. Z. D., Irifune, T., Nishi, M., Tange, Y., Arimoto, T., Shinmei, T., 2016. Phase relations in the
537 system $MgSiO_3$–Al_2O_3 up to 52 GPa and 2000 K. Phys. Earth Planet Inter. 257, 18–27.

538 Liu, Z. D., Ishii, T., Katsura, T., 2017a. Rapid decrease of $MgAlO_{2.5}$ component in bridgmanite with
539 pressure, Geochem. Perspect. Lett. 5, 12-18

540 Liu, Z. D., Nishi. M., Ishii, T., Fei, H. Z., Miyajima, N., Boffa Ballaran, T., Ohfuji, H., Sakai, T., Wang,
541 L., Shcheka, S., Arimoto, T., Tange, Y., Higo, Y., Irifune, T., Katsura, T., 2017b. Phase relations
542 in the system $MgSiO_3$–Al_2O_3 up to 2300 K at lower-mantle pressures. J. Geophys. Res. 10, 7775-
543 7788.

544 McCammon, C. A. (1997). Perovskite as a possible sink for ferric iron in the lower mantle. Nature 387,
545 694–696.

546 Murakami, M., Hirose, K., Yurimoto, H., Nakashima, S., Takafuji, N., 2002. Water in Earth's lower
547 mantle. Science 295, 1885–1887.

548 Navrotsky, A., 1999. A lesson from ceramics. Science 284, 1788–1789.

549 Navrotsky, A., et al. 2003 Aluminum in magnesium silicate perovskite: Formation, structure, and
550 energetics of magnesium-rich defect solid solutions. J. Geophys. Res. 108(7), 2330.

551 Shcheka, S. S., Keppler, H., 2012. The origin of the terrestrial noble-gas signature. Nature 490, 531–
552 534.

553 Stebbins, J. F., Kojitani, H., Akaogi, M., Navrotsky, A., 2003. Aluminum substitution in
554 $MgSiO_3$ perovskite: Investigation of multiple mechanisms by ^{27}Al NMR. Am. Mineral. 88, 1161–
555 1164.

556 Thompson, J. B., 1967. Thermodynamic properties of simple solu-tions. In: P.H. Abelson _Ed..,
557 Research in Geochemistry, Vol. 2, Wiley, New York, pp. 340–361.

558 Walter, M., Kubo, A., Yoshino, T., Brodholt, J., Koga, K. T., Ohishi, Y., 2004. Phase relations and
559 equation-of-state of aluminous Mg-silicate perovskite and implications for Earth's lower mantle.
560 Earth Planet. Sci. Lett. 222, 501–516.

561 Walter, M., Tronnes, R. G., Armstrong, L. S., Lord, O., Caldwell, W. A., Clark, A. M. (2006).
562 Subsolidus phase relations and perovskite compressibility in the system MgO–$AlO_{1.5}$–SiO_2 with
563 implications for Earth's lower mantle. Earth Planet. Sci. Lett. 248:77–89.

564 Xu, Y., McCammon, C. A., Poe, B. T., 1998. The effect of alumina on the electrical conductivity of
565 silicate perovskite. Science 282, 922-924.

566 Xu, J., Yamazaki, D., Katsura, T., Wu, X., Remmert, P., Yurimoto, H., Chakraborty, S., 2011. Silicon
567 and magnesium diffusion in a single crystal of $MgSiO_3$ perovskite. J. Geophys. Res., 116, B12205
568 Yamazaki, D., Kato, T., Yurimoto, H., Ohtani, E., Toriumi, M., 2000. Silicon self-diffusion in $MgSiO_3$
569 perovskite at 25 GPa, Phys. Earth Planet. Inter., 119, 299–309.
570 Yoshino, T., Kamada, S., Zhao, C., Ohtani, E., Hirao, N., 2016. Electrical conductivity model of Al-
571 bearing bridgmanite with implications for the electrical structure of the Earth's lower mantle. Earth
572 Planet. Sci. Lett. 434, 208–219.

573 Zhang, J., Weidner, D. J., 1999. Thermal equation of state of aluminum–enriched silicate perovskite.
574 Science 284, 782–784.

575

576

577

578

579

580

581

582

583

584

585

586

587

588

589

590

591

592

593

594 **Figure and Table captions**

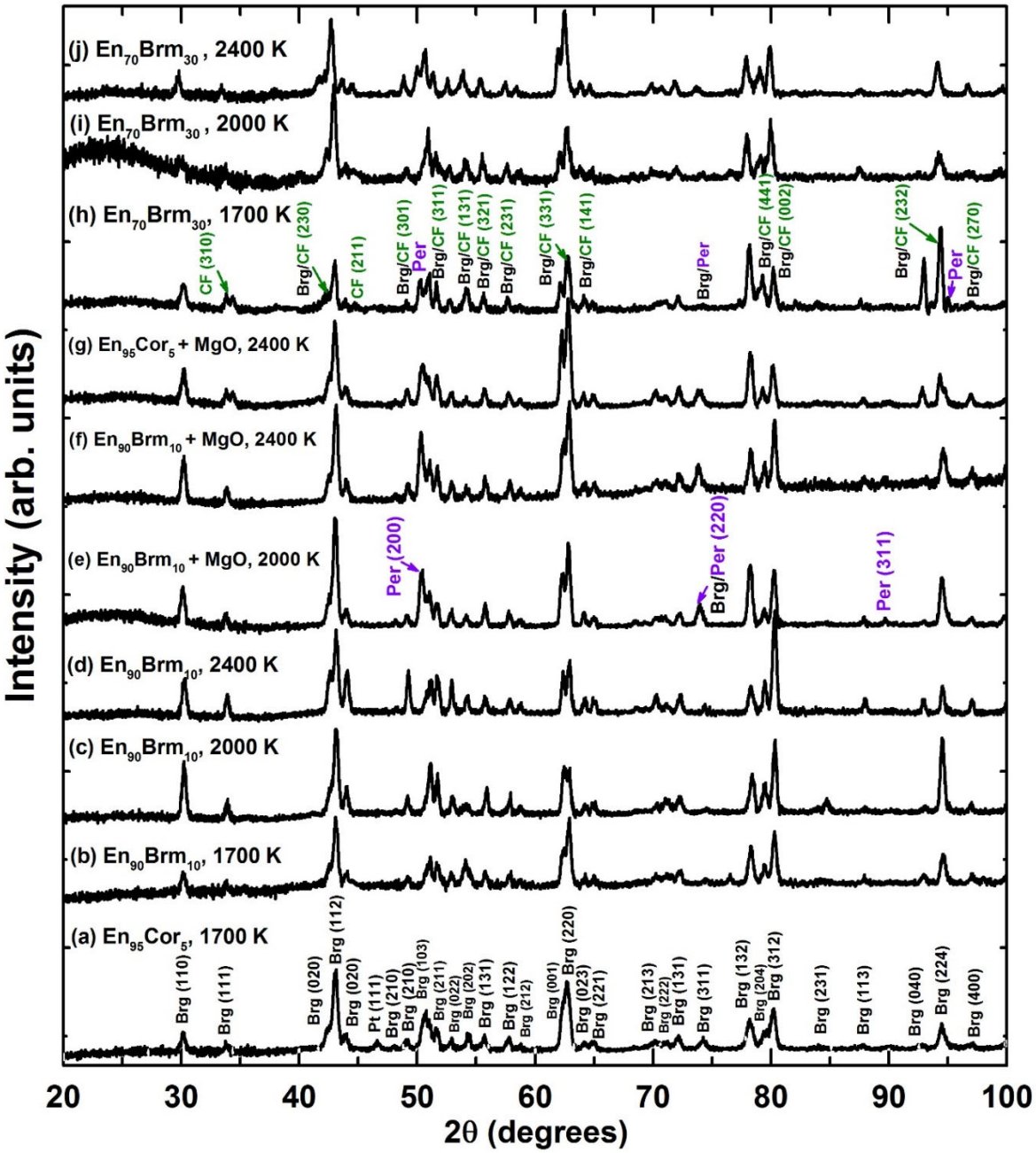

595

596 **Fig. 1.** XRD patterns of run products at 1700, 2000, and 2400 K at a pressure of 27 GPa. The number in parenthesis
597 represents miller induces of the first appearing phase. Abbreviations: Brg, bridgmanite; CF: calcium ferrite-type
598 structure of $MgAl_2O_4$; Per, periclase.

This is an Accepted Manuscript of an article published by Elsevier in Earth and Planetary Science Letters,
available online: https://doi.org/10.1016/j.epsl.2018.10.014

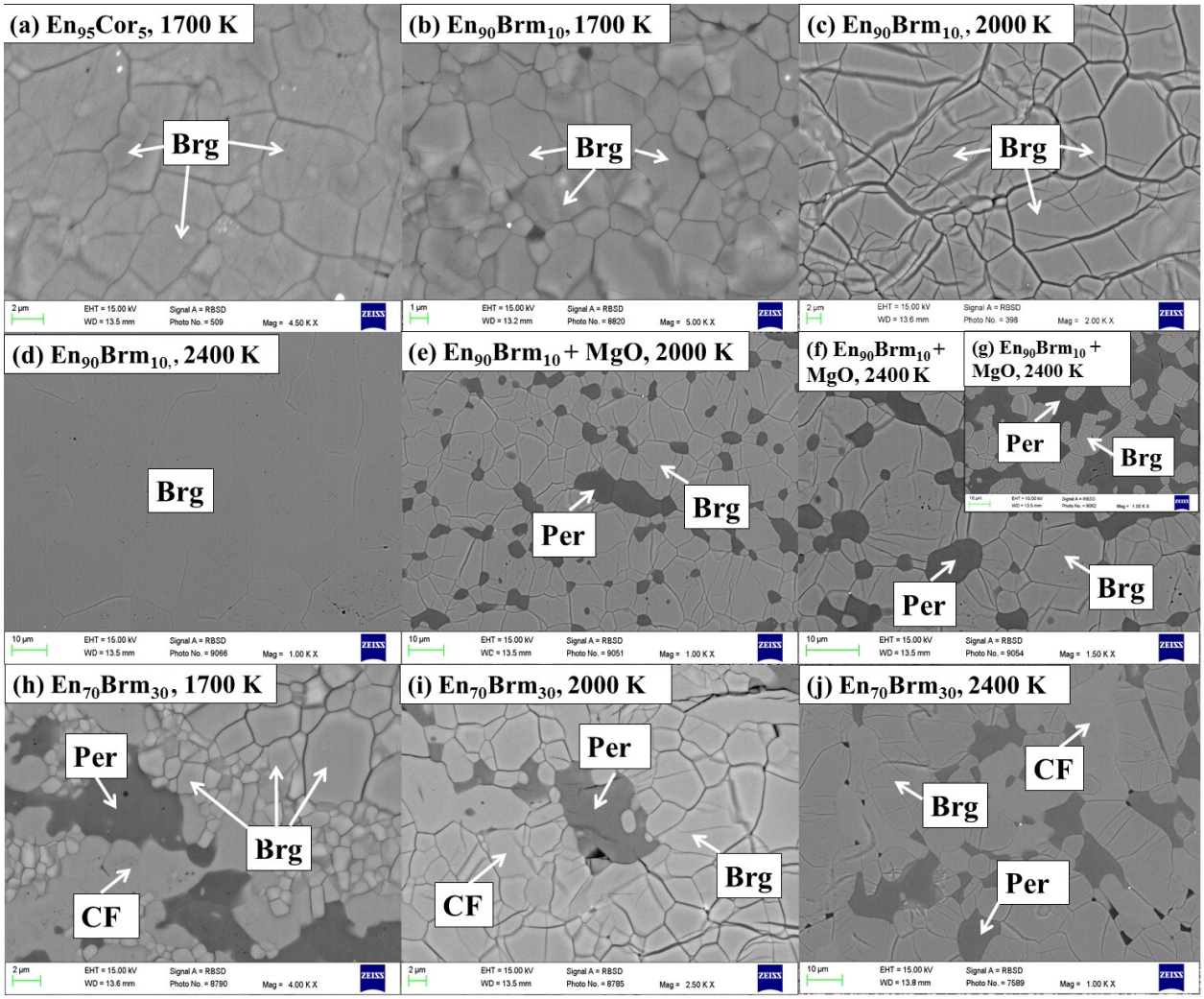

Fig. 2. BSE images of run products at 1700, 2000, and 2400 K under a pressure of 27 GPa. Abbreviations: Brg, bridgmanite; CF: calcium ferrite-type structure of $MgAl_2O_4$; Per, periclase.

This is an Accepted Manuscript of an article published by Elsevier in Earth and Planetary Science Letters,
available online: https://doi.org/10.1016/j.epsl.2018.10.014

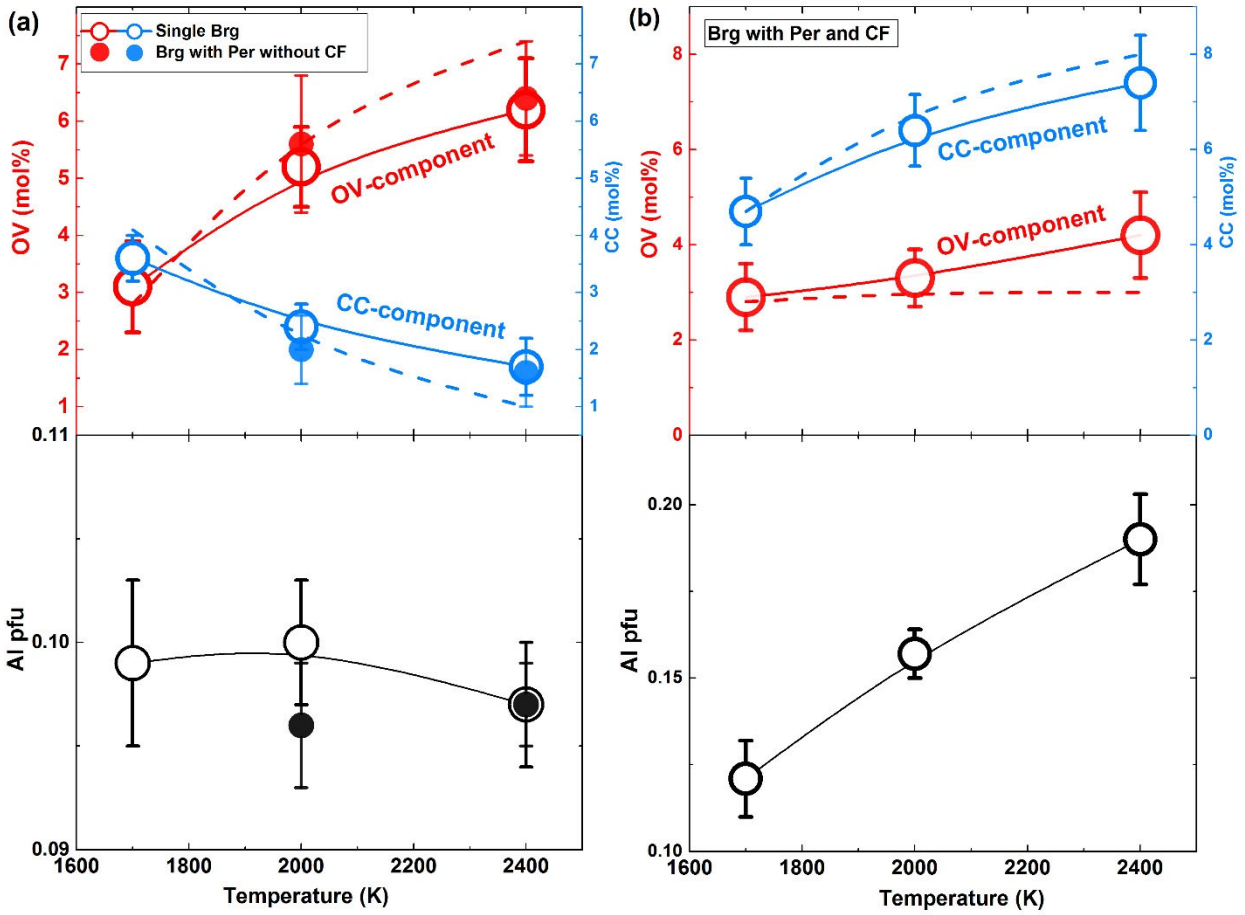

Fig. 3. The content of OV and CC component (upper) and Al pfu (per formula units) (bottom) with temperature for (a) single-phase bridgmanite for $En_{90}Brm_{10}$ (open symbols) and that coexisting with periclase for mixture of $En_{90}Brm_{10}$ and MgO (solid symbols) and (b) bridgmanite coexisting with periclase and CF phase for $En_{70}Brm_{30}$.). Solid lines are the tendency of the experimental data with temperature, while dashed lines are thermodynamic results through a minimum of Gibbs free energy of reaction (1) by $\Delta G_{R1}(P,T,X) = \Delta H_T^0 - T\Delta S_T^0 + \int_{1\,atm}^{P} \Delta V_{P,T} + RT \ln \frac{\left(X_{MgAlO_{2.5}}^{Brg}\right)^2}{\left(X_{MgO}^{Pc}\right)^2 X_{AlAlO_3}^{Brg}} - W_{AlAlO_3}^{Brg}\left(1 - X_{AlAlO_3}^{Brg}\right)^2 + 2W_{MgAlO_{2.5}}^{Brg}\left(1 - X_{MgAlO_{2.5}}^{Brg}\right)^2$ (detailed can be found in Supplementary text and Table S2. Abbreviations: Brg, bridgmanite; CF: calcium ferrite-type structure of $MgAl_2O_4$; Per, periclase; OV: $MgAlO_{2.5}$; CC: $AlAlO_3$.

This is an Accepted Manuscript of an article published by Elsevier in Earth and Planetary Science Letters,
available online: https://doi.org/10.1016/j.epsl.2018.10.014

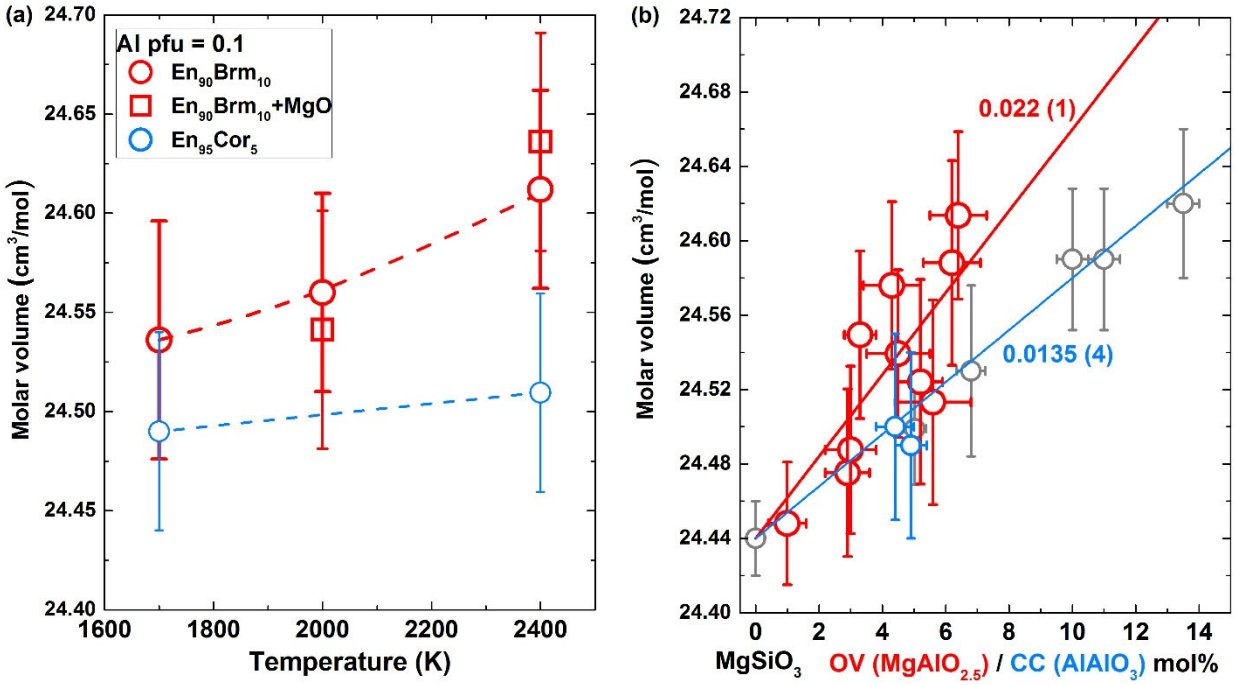

Fig. 4. Molar volume of bridgmanite (a) with an Al pfu of 0.1 as a function of temperature and (b) CC ($AlAlO_3$) or OV ($MgAlO_{2.5}$) in mol%. The number is the linear increase rate for molar volume with CC and OV component and that in parentheses represents the standard deviation of the last digit. Black symbols are data from Liu et al. (2017b). Dashed lines in (a) are the tendency of the data with temperature, while solid lines are linear fitting results.

This is an Accepted Manuscript of an article published by Elsevier in Earth and Planetary Science Letters,
available online: https://doi.org/10.1016/j.epsl.2018.10.014

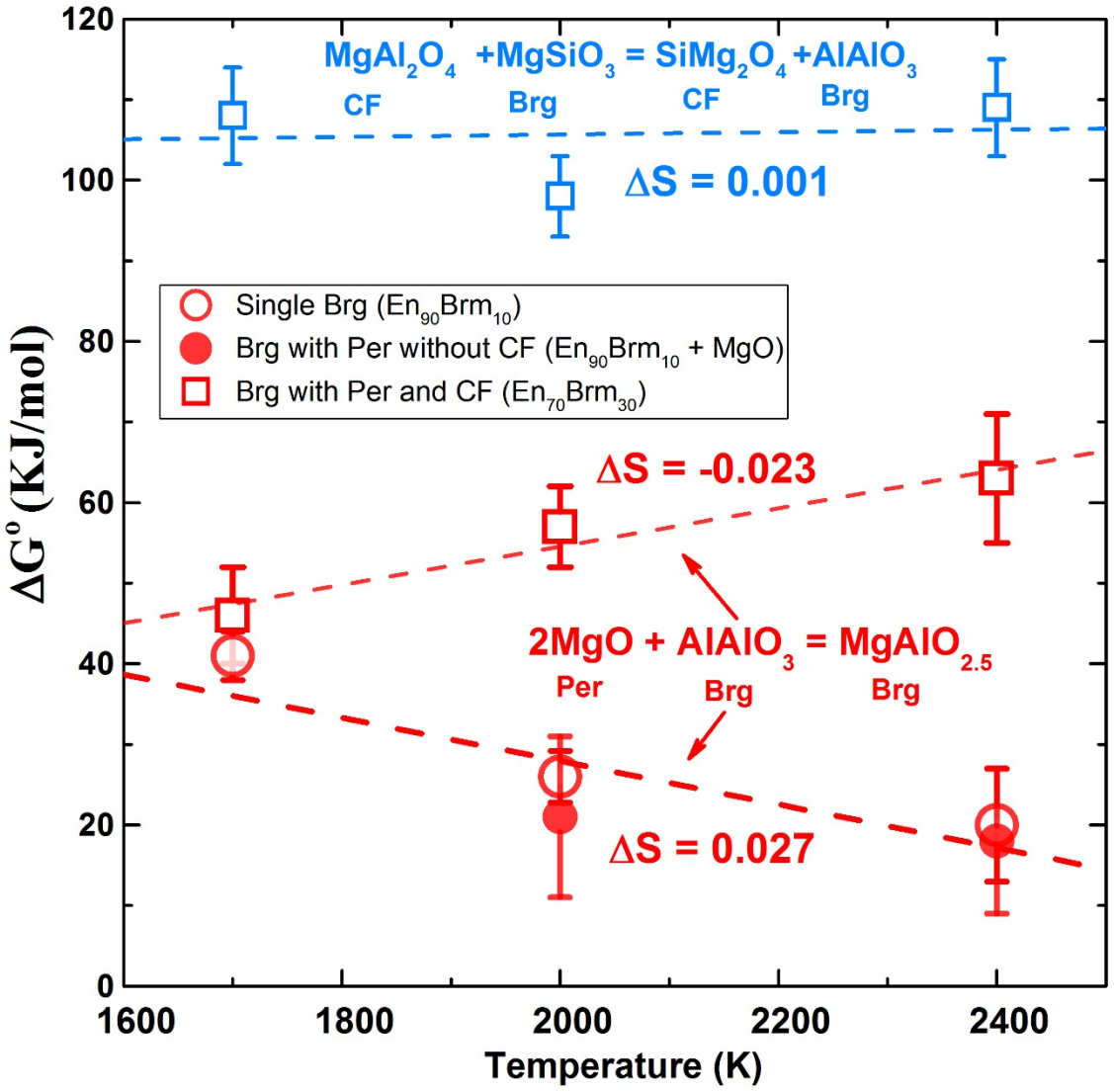

637

638 **Fig. 5.** Gibbs free energy of reaction (1) for single-phase bridgmanite for $En_{90}Brm_{10}$ (red open circles),
639 bridgmanite coexisting with periclase for mixture of $En_{90}Brm_{10}$ and MgO (red solid circles) and bridgmanite with
640 periclase and CF-phase from $En_{70}Brm_{30}$ (red squires), and that of reaction (12) for bridgmanite coexisting with
641 periclase and CF phase for $En_{70}Brm_{30}$ (blue squires). Dashed lines are the linear fitting results ($\Delta G = \Delta H - T\Delta S$)
642 and the slope is ΔS. Abbreviations: Brg, bridgmanite; CF: calcium ferrite-type structure of $MgAl_2O_4$; Per,
643 periclase.

644 **Table 1**. Experimental conditions and run products.

Run No.	Start Comp.	P (GPa) / T (K) / t (hours)	Phases
IRIS506	$En_{90}Brm_{10}$	27 /1700 /30	Brg
	$En_{70}Brm_{30}$	–	Brg + CF + Per
	$En_{95}Cor_5$	–	Brg
IRIS420	$En_{90}Brm_{10}$	27 / 2000 /20	Brg
	$En_{90}Brm_{10}$ + MgO	–	Brg + Per
	$En_{70}Brm_{30}$	–	Brg + CF + Per
IRIS512	$En_{90}Brm_{10}$	27 /2400 /4	Brg
	$En_{90}Brm_{10}$ + MgO	–	Brg + Per
	$En_{70}Brm_{30}$	–	Brg + CF + Per
IRIS527	$En_{95}Cor_5$	27 /2400 /6	Brg
	$En_{95}Cor_5$ + MgO	–	Brg + Per

645 –: the same as the above conditions.

646 Abbreviations: Brg, bridgmanite; CF: calcium ferrite-type structure of $MgAl_2O_4$; Per, periclase.

647

648

649

650

651

652

653

654

655

656

657

658

659

660 **Table 2**. The compositions of the run products. Oxide analyses are reported in wt%. The total number of cations for bridgmanite, CF-phase, and
661 periclase is normalized to two, three, and one, respectively. Number in parentheses represents standard deviations for the last digit (s).

Start Comp.	Phases	MgO	Al_2O_3	SiO_2	Total	Mg	Al	Si	O	Brg			CF	
										OV (mol%)	CC (mol%)	En (mol%)	$Mg(MgSi)O_4$ (mol%)	$MgAl_2O_4$ (mol%)
IRIS506 (1700 K)														
$En_{95}Cor_5$	Brg [n = 35]	38.68 (56)	5.01 (13)	57.71 (48)	101.39 (86)	0.951 (7)	0.097 (2)	0.952 (7)	3.000 (7)	-0.1 (14)	4.9 (7)	95.2 (7)		
$En_{70}Brm_{30}$	Brg [n = 28]	39.05 (46)	6.27 (55)	56.46 (70)	99.17 (59)	0.954 (6)	0.121 (11)	0.925 (7)	2.986 (3)	2.9 (7)	4.6 (6)	92.5 (7)		
	CF [n = 8]	35.14 (77)	53.29 (97)	10.24 (59)	98.67 (65)	1.253 (17)	1.502 (28)	0.245 (14)	3.996 (7)				24 (1)	76 (2)
	Per [n = 5]	99.44 (56)	0.22 (2)		99.67 (67)	0.998 (0)	0.002 (0)		1.001 (0)					
$En_{90}Brm_{10}$	Brg [n = 55]	39.46 (30)	5.14 (15)	56.99 (64)	101.59 (70)	0.965 (4)	0.099 (3)	0.935 (4)	2.985 (4)	3.0 (8)	3.5 (4)	93.5 (4)		
IRIS420 (2000 K)														
$En_{90}Brm_{10}$	Brg [n = 20]	39.38 (31)	5.12 (18)	55.55 (36)	100.05 (52)	0.976 (4)	0.100 (3)	0.924 (4)	2.974 (4)	5.2 (7)	2.4 (4)	92.4 (4)		
$En_{70}Brm_{30}$	Brg [n = 30]	38.08 (28)	8.31 (38)	54.76 (47)	101.15 (72)	0.936 (4)	0.161 (7)	0.903 (5)	2.983 (5)	3.3 (5)	6.4 (4)	90.3 (6)		
	CF [n = 10]	37.40 (35)	46.26 (73)	14.78 (50)	98.43 (50)	1.338 (12)	1.308 (19)	0.355 (12)	4.009 (6)				36 (1)	64 (1)
	Per [n = 5]	99.37 (69)	0.81 (6)		100.81 (67)	0.994 (1)	0.006 (0)		1.003 (0)					
$En_{90}Brm_{10}$ + MgO	Brg [n = 26]	40.45 (32)	4.99 (9)	56.87 (37)	102.31 (70)	0.980 (6)	0.096 (2)	0.924 (6)	2.972 (6)	5.6 (12)	2.0 (6)	92.4 (6)		
	Per [n = 5]	99.91 (16)	0.79 (3)	0.05 (1)	100.75 (14)	0.993 (0)	0.006 (1)		1.003 (0)					
IRIS512 (2400 K)														
$En_{70}Brm_{30}$	Brg [n = 40]	37.30 (32)	9.66 (67)	53.03 (68)	100.03(98)	0.927 (8)	0.190 (13)	0.884 (7)	2.979 (5)	4.3 (9)	7.3 (8)	88.4 (8)		
	CF [n = 10]	38.84 (77)	43.86(56)	16.17 (51)	98.87 (104)	1.381 (16)	1.233 (22)	0.386 (9)	4.002 (6)				39 (1)	61 (1)
	Per [n = 5]	98.18 (56)	1.30 (5)	0.03 (1)	99.51 (62)	0.990 (0)	0.010 (0)		1.005 (0)					
$En_{90}Brm_{10}$	Brg [n = 40]	40.19 (39)	5.02 (13)	56.11 (61)	101.31 (85)	0.983 (5)	0.097 (3)	0.920 (5)	2.969 (5)	6.2 (9)	1.7 (5)	92.0 (5)		
$En_{90}Brm_{10}$ + MgO	Brg [n = 26]	40.09 (32)	4.98 (14)	55.89 57)	100.95 (62)	0.984 (6)	0.097 (3)	0.920 (5)	2.968 (5)	6.4 (9)	1.6 (5)	92.0 (5)		
	Per [n = 5]	98.23 (41)	1.20 (7)	0.05 (1)	99.47 (39)	0.991 (1)	0.009 (1)		1.005 (0)					
IRIS527 (2400 K)														
$En_{95}Cor_5$ + MgO	Brg [n = 25]	40.15 (47)	4.89 (35)	57.09 (42)	102.13 (69)	0.975 (5)	0.094 (7)	0.931 (7)	2.978 (5)	4.5 (10)	2.5 (5)	93.0 (7)		
	Per [n = 4]	98.30 (49)	1.14 (11)	0.34 (30)	99.78 (19)	0.989 (2)	0.009 (0)	0.002 (2)	1.007 (2)					
$En_{95}Cor_5$	Brg [n = 10]	39.19 (38)	5.06 (12)	57.83 (47)	102.07 (76)	0.956 (3)	0.098 (3)	0.946 (3)	2.995 (3)	1.0 (6)	4.4 (3)	94.6 (3)		

662 Abbreviations: Brg, bridgmanite; CF: calcium ferrite-type structure of $MgAl_2O_4$; Per, periclase; OV: $MgAlO_{2.5}$; CC: $AlAlO_3$; En: $MgSiO_3$.

663 n is the number of analyses.

Supplementary Material

Introduction

This Supplementary Material provides the Gibbs free energy calculation (Text), Lattice parameters of synthetic aluminous bridgmanite (Table S1), elastic parameters of bridgmanite used for the minimum Gibbs free energy calculation combined with Eq. (9) in the main text (Table S2), and references.

Text

Gibbs free energy for reaction (1): 2MgO + $AlAlO_3$ (CC) = 2$MgAlO_{2.5}$ (OV) at high pressure and high temperature can be expressed as:

$$\Delta G_{R1}(P,T,X) = \Delta H_T^0 - T\Delta S_T^0 + \int_{1\ atm}^{P} \Delta V_{P,T} + RT \ln \frac{\left(X_{MgAlO_{2.5}}^{Brg}\right)^2}{\left(X_{MgO}^{Pc}\right)^2 X_{AlAlO_3}^{Brg}} - W_{AlAlO_3}^{Brg}\left(1 - X_{AlAlO_3}^{Brg}\right)^2 + 2W_{MgAlO_{2.5}}^{Brg}\left(1 - X_{MgAlO_{2.5}}^{Brg}\right)^2 \quad \text{(S1)}$$

where ΔH_T^0 is the enthalpy; ΔS_T^0 is the entropy; T is temperature; P is the pressure; $\Delta V_{P,T}$ is the molar volume at *HP-HT*; $X_{MgAlO_{2.5}}^{Brg}$ and $X_{AlAlO_3}^{Brg}$, respectively, are the mole fraction of the $MgAlO_{2.5}$ and $AlAlO_3$ components in the bridgmanite; $W_{AlAlO_3}^{Brg}$ and $W_{MgAlO_{2.5}}^{Brg}$ are interaction parameters for the degree of the non-ideality of mixing.

The enthalpy and entropy change at T can be obtained by:

$$\Delta H_T^0 = \Delta H_{T_0}^0 + \int_{T_0}^{T} \Delta C_P dT \quad \text{(S2)}$$

$$\Delta S_T^0 = \Delta S_{T_0}^0 + \int_{T_0}^{T} (\Delta C_P/T) dT \quad \text{(S3)}$$

where $\Delta H_{T_0}^0$ and $\Delta S_{T_0}^0$ are the entralpy and entropy changes at 298 K at room pressure, respectively, and ΔC_P is the heat capacity difference. ΔC_P can be expressed as:

$$\Delta C_P = A + BT^{-0.5} + CT^{-2} \quad \text{(S4)}$$

where A, B, and C are constants. The effect of T and P on molar volume can be got by the following equations:

$$V_T^0 = V_{T_0}^0 \exp\left(\int_{298}^{T} \alpha_T dT\right) \quad \text{(S5)}$$

$$\alpha_T = a_0 + a_1 T + a_2 T^{-2} \quad \text{(S6)}$$

Where V_T^0 and $V_{T_0}^0$ are the molar volume at T and 298 K at room pressure, respectively, and a_0, a_1, and a_2 are constants. After that, the molar volume at high pressure can be obtained by using the third order Birch-Murnaghan equation:

$$P = \frac{3}{2} K_T \left\{ \left(\frac{V_{T_0}^0}{V} \right)^{\frac{7}{3}} - \left(\frac{V_{T_0}^0}{V} \right)^{\frac{5}{3}} \right\} \left\{ 1 - \frac{3}{4} (4 - K') \left[\left(\frac{V_{T_0}^0}{V} \right)^{\frac{2}{3}} - 1 \right] \right\} \quad \text{(S7)}$$

where K_T and K', respectively, are the bulk modulus and its pressure derivative, and V is the molar volume at *HP-HT*. The temperature dependence of K_T can be calculated as:

$$K_T = K_0 + \left(\frac{\partial K}{\partial T} \right)_P (T - 298) \quad \text{(S8)}$$

where K_0 is the bulk modulus at ambient conditions and $\left(\frac{\partial K}{\partial T} \right)_P$ is the temperature derivative of K_T. The used elastic parameters are listed in Table S2.

Table S1. Lattice parameters of synthetic aluminous bridgmanite.

Run No.	Comp. of Brg	a (Å)	b (Å)	c (Å)	V (Å^3)	Molar volume (cm^3/mol)
IRIS420	2000 K					
	$Mg_{0.976}Al_{0.100}Si_{0.924}O_{2.974}$	4.773 (3)	4.935 (5)	6.925 (5)	163.12 (31)	24.55 (6)
	$Mg_{0.936}Al_{0.161}Si_{0.903}O_{2.983}$	4.778 (2)	4.949 (7)	6.921 (4)	163.66 (36)	24.63 (5)
	$Mg_{0.980}Al_{0.097}Si_{0.924}O_{2.972}$	4.771 (1)	4.939 (8)	6.918 (5)	163.01 (46)	24.53 (6)
IRIS506	1700 K					
	$Mg_{0.951}Al_{0.094}Si_{0.952}O_{3.000}$	4.774 (2)	4.930 (7)	6.911 (4)	162.67 (48)	24.48 (7)
	$Mg_{0.965}Al_{0.099}Si_{0.935}O_{2.985}$	4.770 (3)	4.934 (3)	6.919 (5)	162.84 (35)	24.51 (4)
	$Mg_{0954}Al_{0.121}Si_{0.925}O_{2.986}$	4.774 (1)	4.935 (1)	6.917 (2)	162.98 (45)	24.53 (5)
IRIS512	2400 K					
	$Mg_{0.983}Al_{0.097}Si_{0.920}O_{2.969}$	4.776 (2)	4.942 (3)	6.924 (3)	163.48 (31)	24.60 (6)
	$Mg_{0.984}Al_{0.097}Si_{0.920}O_{2.968}$	4.780 (3)	4.940 (3)	6.930 (4)	163.64 (30)	24.63 (7)
	$Mg_{0.927}Al_{0.190}Si_{0.884}O_{2.979}$	4.775 (1)	4.949 (7)	6.936 (2)	163.92 (49)	24.67 (5)
IRIS527	$Mg_{0.956}Al_{0.098}Si_{0.946}O_{2.995}$	4.776 (2)	4.926 (4)	6.920 (2)	162.80 (31)	24.51 (5)
	$Mg_{0.975}Al_{0.094}Si_{0.931}O_{2.978}$	4.773 (2)	4.942 (8)	6.920 (2)	163.23 (54)	24.57 (4)

Number in parentheses represents standard deviation and is placed in the last digit (s).

Table S2. Elastic parameters of bridgmanite used for the minimum Gibbs free energy calculation combined with Eq. (9) in the main text.

Phase	$MgSiO_3$-Brg	$AlAlO_3$-Brg	$MgAlO_{2.5}$-Brg	MgO
V_0 (cm^3/mol)	24.44 [a]	25.79 (5) (This study)	26.64 (10) (This study)	11.27 (1)[h]
H_0 (KJ/mol)	10.79 (196)[b]	142.3 [b]	142.3 [b]	36.48 (50)[i]
S_0 (J/mol)	57 (1)[c]	60 (1)[b]	70 [&]	26.92[i]
K_0 (GPa)	257 (1)[a]	261[a]	155[g]	160.9[i]
K_0'	4.09 (6)[a]	4[d]	4[#]	4.35 (10) [h]
$(\partial K_T/\partial T)_P$ (GPa/K)	-0.035 (2)[d]	-0.057 (5)[f]	-0.057 (5)[#]	-0.0272 [h]
$\alpha_T = a_0 + a_1 T + a_2 T^{-2}$ (K^{-1})				
$a_0 \times 10^5$	1.982[e]	2.08 (26) [f]	2.08 (26) [#]	3.38[i]
$a_1 \times 10^8$	0.818[e]	2.21 (67) [f]	2.21 (67) [#]	12.52[i]
$a_2 \times 10$	-4.740[e]	0	0	-19.13[i]
$C_P = A + BT^{-0.5} + CT^{-2}$ (K^{-1})				
$A \times 10^{-2}$	1.769[e]	1.769*	1.769*	0.6[i]
$B \times 10^{-3}$	-1.565[e]	-1.565*	-1.565*	-0.36[i]
$C \times 10^{-6}$	0	0	0	-0.61[i]

a: Tange et al. (2012)
b: Akaogi and Ito (1999)
c: Akaogi and Ito (1993)
d: Katsura et al. (2009)
e: Funamori et al. (1996)
f: Zhand and Wiedner (1999)
g: Brodholt (2000)
h: Kono et al. (2010)
i: Kojitani et al. (2012)
j: Kojitani et al. (2007)
*: the same value with that of $MgSiO_3$-Brg
#: the same value of that of CC-Brg
&: estimated from the entropy change from the present study
Abbreviations: Brg: bridgmanite; OV: $MgAlO_{2.5}$; CC: $AlAlO_3$;
Number in parentheses represents standard deviation and is placed in the last digit (s).

Reference:

Akaogi, M., Ito, E. (1993) Heat capacity of $MgSiO_3$ perovskite. Geophysics Research Letter, 20, 105-108.

Akaogi, M., Ito, E. (1999) Calorimetric study on majorite–perovskite transi - tion in the system $Mg_4Si_4O_{12}$-$Mg_3Al_2Si_3O_{12}$: transition boundaries with positive pressure-temperature slopes. Physics of the Earth and Planetary Interiors 114, 129–140.

Brodholt, J. P., 2000. Pressure-induced changes in the compression mechanism of aluminous perovskite in the Earth's mantle, Nature 407, 620–622.

Funamori, N., Yag i, T., Utsum i, W., Kond o , T., Uchida, T., Funamori, M. (1996) Thermoelastic properties of $MgSiO_3$ perovskite determined by in situ X ray observations up to 30 GPa and 2000 K. Journal of Geophysical Research 101, 8257–8269.

Katsura, T., Yokoshi, S., Kawabe, K., Shatskiy, A., Manthilake, M. Zhai, S. M., Fukui, H., Hegoda, H., Yoshino, T., Yamazaki, D., Matsuzaki, T., Yoneda, A., Ito, E., S u gita, M., To miok a, N., Hagiya, K., Nozawa, A., Fun akoshi, K. (2009) P-V-T relations of $MgSiO_3$ perovskite determined by in situ X-ray diffraction using a large-volume high-pressure apparatus. Geophysical Research Letters 36, L01305.

Kojitani, H., R. Hisatomi, Akaogi, M. (2007) High-pressure phase relations and crystal chemistry of calcium ferrite-type solid solutions in the system $MgAl_2O_4$-Mg_2SiO_4, American Mineralogist *92*, 1112-1118.

Kojitani, H., I s hii, T., Akaogi, M. (2012) Thermodynamic investigation of phase equilibrium boundary between calcium ferrite-type $MgAl_2O_4$ and $MgO + Al_2O_3$. Physics of the Earth and Planetary Interiors 212–213, 100–105.

Kono, Y., Irifune , T., Higo , Y., Inoue, T., Barnhoorn, A. (2010) PVT relation of MgO derived by simultaneous elastic wave velocity and in situ X-ray measurements: A new pressure scale for the mantle transition region. Physics of the Earth and Planetary Interiors 183, 196–21.

Tange, Y., Kuwayama, Y., Irifune , T., Funakosh i, K.- i., Ohishi , Y. (2012) P-V-T equation of state of $MgSiO_3$ perovskite based on the MgO pressure scale: A comprehensive reference for mineralogy of the lower mantle. Journal of Geophysical Research 117, B06201.

Zhang, J., Weidner, D. J., 1999. Thermal equation of state of aluminum enriched silicate perovskite, Science 284, 782–784.